DOI: 10.1109/LCOMM.2020.3013171

On the Impact of Residual Transceiver Impairments in mmWave RF Beamforming Systems

Author 1, Author 2, and Author 3

***Abstract*—Millimeter wave (mmWave) communication has emerged as a key technology for achieving high data-rates and low latency in 5G networks. Radio-frequency (RF) or analog beamforming is used to provide additional (beamforming) gain to compensate for propagation phenomena in the mmWave spectrum. In this letter, we analyzed the effects of residual transceiver impairments on the performance of a single-user mmWave RF beamforming system. We derived the closed-form expressions of the ergodic capacity in both Line-of-Sight (LoS) and Non-Line-of-Sight (NLoS) channels. The derived formulas are applicable for both perfect and codebook-based beam alignment. In the former, they are exact, while in the latter are approximate, but with a high degree of accuracy. The theoretical findings are verified by Monte-Carlo simulations showing an excellent agreement.**

***Index Terms*—Beamforming, mmWave, impairments, RF.**

I. Introduction

During the last decade, we are witnessing increased demands for data rates and the shortage of spectrum in particular for Sub-6 GHz links. This has motivated the research community to explore new frequency bands that offer significant improvements of communication bandwidth. In this context, millimeter wave (mmWave) communication has been recognized as a candidate technology for achieving high data rates and low latency in 5G wireless networks [1].

The mmWave spectrum, however, brings along technical difficulties and physical phenomena that limit the desired capacity. The mmWave channel is directional with limited scattering, and it is characterized by high attenuation and absorption losses [2]. Beamforming creates transmit and receive beamforming gains to obtain a high enough signal-to-noise ratio (SNR) for signal reception [3]. This is supported by the use of small wavelengths, which allow a high number of antennas to be densely packed to form large arrays. Furthermore, large signal bandwidths require very high sample rates, requiring the involvement of high cost and power-hungry analog-to-digital converters (ADC). This limits the number of radio-frequency (RF) chains mmWave transmitters and receivers can feature. This, in turn, imposes some constraints on beamformer types.

Motivated by the above, a lot of research work in recent years has been devoted to different aspects of mmWave beamforming communications. Some of these cover, for instance, system performance analysis [4], [5], channel estimation techniques [6], beam training algorithms [7], [8], codebook design [9], beam tracking algorithms [10], hybrid beamforming architectures and algorithms [11], [12], etc. However, less work has been devoted to the performance analysis of mmWave RF beamforming systems subject to transceiver impairments from the *information-theoretic* point of view. In one such example [13], the authors have studied transmitter impairments and derived an upper bound for the capacity of a mmWave RF beamforming system in a Non-Line-of-Sight (NLoS) channel.

Author 1 and Author 2 are with xyz (e-mails: author1, author2@xyz).
Author 3 is with xyz, and also with uvw (e-mail: author3@xyz).

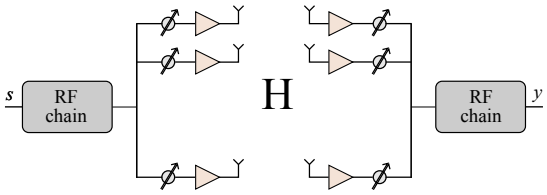

Fig. 1. An illustration of a mmWave RF beamforming system.

In this Letter, we derived the exact analytical expressions of the ergodic capacity of a mmWave RF beamforming system. The theoretical analysis covers both Line-of-Sight (LoS) and NLoS channels and incorporates the effects of residual transmitter and receiver impairments. The closed-form expressions are then verified via Monte-Carlo simulations.

This rest of the Letter is structured as follows: Section II introduces the system, channel, and impairment models. Analytical derivations are presented in Section III, whereas both theoretical and numerical results are covered in Section IV. The conclusion is given in Section IV.

II. System, Channel and Impairment Models

A. System Model

We consider a mmWave RF beamforming system featuring uniform linear antenna arrays (ULAs) at both transmitter and receiver, as shown in Fig. 1. The transmitter has N_{t} antennas, and the receiver uses N_{r} antennas for signal reception. A single RF chain is considered. Assuming perfect synchronization, and a transmitted symbol s with the unit power $P_s = 1$, the received signal is [9]

$$y = \sqrt{\rho}\mathbf{w}^H\mathbf{H}\mathbf{f}s + \mathbf{w}^H\mathbf{n}, \tag{1}$$

where ρ represents the average received power, $\mathbf{f}$ and $\mathbf{w}$ are the unit norm transmit and receive beamforming vectors, respectively, $\mathbf{H} \in \mathbb{C}^{N_{\mathrm{r}} \times N_{\mathrm{t}}}$ is the channel matrix, and $\mathbf{n}$ is the additive Gaussian noise vector satisfying $\mathbb{E}\left[\mathbf{n}\mathbf{n}^H\right] = \sigma_n^2\mathbf{I}_{\mathbf{N_r}}$.

Owing to (1), the received SNR is

$$\mathrm{SNR} = \mathrm{SNR}_0|\mathbf{w}^H\mathbf{H}\mathbf{f}|^2, \tag{2}$$

with $\mathrm{SNR}_0 = \frac{\rho}{\sigma_n^2}$. To maximize (2), a joint Tx/Rx beamforming is performed as

$$arg\max_{\mathbf{w},\mathbf{f}} \quad |\mathbf{w}^H\mathbf{H}\mathbf{f}|^2. \tag{3}$$

If $\mathbf{H}$ is known, the optimal $\mathbf{w}$ and $\mathbf{f}$ are found by the singular value decomposition (SVD) [9]. Otherwise, the transmitter and the receiver sense the channel by testing the beamforming vectors from their respective codebooks (*i.e.* $\mathbf{w} \in W, \mathbf{f} \in F$), and select a pair of beamforming vectors that maximizes (3).

Denoting h_{eff} the effective channel obtained after the joint Tx/Rx beamforming in (3), (1) can be rewritten as

$$y = \sqrt{\rho} h_{\text{eff}} s + n_{\text{eff}}, \tag{4}$$

where n_{eff} is the effective noise, satisfying $\mathtt{E}\left[n_{\text{eff}} n_{\text{eff}}^H\right] = \sigma_n^2$. Now, the ergodic capacity is given by [17]

$$R = \mathtt{E}\left\{\log_2\left(1 + \text{SNR}_0 \left|h_{\text{eff}}\right|^2\right)\right\}. \tag{5}$$

B. Channel Model

We adopt the L-scatter channel model [9], expressed as

$$\mathbf{H} = \sqrt{\gamma N_{\text{r}} N_{\text{t}}} \sum_{p=0}^{L-1} \alpha_p \mathbf{a}_{\text{r}}(\theta_p) \mathbf{a}_{\text{t}}(\phi_p)^H, \tag{6}$$

where L is the number of resolvable paths corresponding to the limited number of scatters, $\alpha_p \sim \mathcal{CN}(0, \sigma_p^2)$ is the gain of the p-th path, while ϕ_p and θ_p are the normalized angles of departure and arrival (AoDs/AoAs) in azimuth, respectively. $\gamma = \left(\sum_{p=0}^{L-1} \mathtt{E}(|\alpha_p|^2)\right)^{-1}$ is the power normalization factor to (6). The normalized AoDs and AoAs are in the range [-1, 1], and are related to the physical AoDs and AoAs as $\phi_p = \frac{2d}{\lambda}\sin(\Phi_p)$ and $\theta_p = \frac{2d}{\lambda}\sin(\Theta_p)$, where λ is the carrier wavelength and $d = \lambda/2$ is the spacing between adjacent antennas. The physical AoDs and AoAs are in the range [-$\pi/2$, $\pi/2$]. $\mathbf{a}_{\text{r}}$ and $\mathbf{a}_{\text{t}}$ are the array response vectors at the transmitter and the receiver, respectively. For an ULA with N antennas, the array response vector is given by [9]

$$\mathbf{a}(\phi) = \frac{1}{\sqrt{N}}\left[1, e^{j\pi\phi}, ..., e^{j(N-1)\pi\phi}\right]. \tag{7}$$

An extension to a planar array is straightforward.

With the channel model in (6), both LoS and NLoS channels can be considered. In a LoS channel, there is a dominant path. Typically, one sets the first path to be the LoS with a variance of σ_0^2 and random AoD and AoA. The remaining paths are NLoS, having, for instance, 10-20 dB smaller variance (*i.e.* $\sigma_1^2 = \sigma_2^2 = ... = \sigma_{L-1}^2 = \sigma_0^2/A$, being A the attenuation factor) and random AoDs and AoAs. The aim of the joint Tx/Rx beamforming is to find the best path, *i.e.* the LoS path. In an NLoS channel, all paths are NLoS and, typically, have the same variance (*i.e.* $\sigma_0^2 = \sigma_1^2 = ... = \sigma_{L-1}^2 = \sigma^2$), and random AoDs and AoAs. In this case, an arbitrary strong path can be feasible during the joint Tx/Rx beamforming.

C. Residual Impairments Model

Practical communication systems suffer from hardware impairments. Ideally, the effect of these impairments should be investigated jointly, although they can be analyzed separately [14]. Compensation schemes are often applied, leading to a residual distortion noise (see [15] and references therein) that can be approximated by independent additive distortion noise at both transmitter and receiver [15].

By virtue of [15], and building on (4), the system model that includes residual hardware impairment due to transmitter and receiver is given by

$$y = \sqrt{\rho} h_{\text{eff}}(s + \eta_{\text{t}}) + \eta_{\text{r}} + n_{\text{eff}}, \tag{8}$$

where η_{t} and η_{r} represent the residual distortion noises and, according to [15], are modeled by

$$\eta_{\text{t}} \sim \mathcal{CN}(0, \kappa_{\text{t}}^2 P_s) \quad \eta_{\text{r}} \sim \mathcal{CN}(0, \rho\kappa_{\text{r}}^2 |h_{\text{eff}}|^2 P_s). \tag{9}$$

The parameters κ_{t} and κ_{r} define the level of Tx and Rx impairments, respectively. These are connected to the error vector magnitude (EVM), which is a figure of merit of an RF transceiver. The transmitter EVM is defined by [15]

$$EVM = \sqrt{\frac{\mathtt{E}_{\eta_{\text{t}}}(|\eta_{\text{t}}|^2)}{\mathtt{E}_s(|s|^2)}} = \kappa_{\text{t}}. \tag{10}$$

According to the IEEE 802.11ad standard [16], single-carrier (SC) mode, the transmitter EVM is specified in the range from -21 to -6 dB, which sets $\kappa_{\text{t}} \in [0.089, 0.5]$. By regrouping the terms in (8), a joint Tx and Rx distortion noise, $\Delta \sim \mathcal{CN}\left(0, \rho\kappa^2 |h_{\text{eff}}|^2\right)$ is defined, where $\kappa = \sqrt{\kappa_{\text{t}}^2 + \kappa_{\text{r}}^2}$ denotes the level of joint Tx and Rx impairments.

The ergodic capacity can now be expressed as

$$R = \mathtt{E}\left\{\log_2\left(1 + \frac{|h_{\text{eff}}|^2}{|h_{\text{eff}}|^2\kappa^2 + \text{SNR}_0{}^{-1}}\right)\right\}. \tag{11}$$

If $\kappa = 0$ (*i.e.* an ideal system) is set in (11), (5) is obtained.

III. Analytical Derivation

A. Derivation of $|h_{\text{eff}}|^2$ Statistics

To solve the expectation in (11), the statistics of $|h_{\text{eff}}|^2$ is required. The statistics are driven by the channel sensing process in the joint Tx/Rx beamforming. To detect AoDs (or AoAs), we select $N(= N_t$ or $N_r)$ beamforming vectors to cover the range $[-\pi/2, \pi/2]$. Basically, we uniformly quantize the range of $sin(\phi)$, *i.e.* [-1, 1], into N bins and use the angle corresponding to the center of each bin as the beamforming direction. Thus, the beamforming vectors are designed as

$$\mathbf{w}_i, \mathbf{f}_i = \mathbf{a}\left(\varphi_i\right), \varphi_i = -1 + \frac{2i+1}{N}, i = 0, ..., N-1. \tag{12}$$

Let us now concentrate, for instance, on the 0-th path and assume that its AoD falls in the *i*-th bin of the Tx and its AoA in the *j*-th bin at the Rx side. The effective channel gain w.r.t. $\mathbf{w}_j$,$\mathbf{f}_i$ reads

$$|\mathbf{w}_j^H \mathbf{H} \mathbf{f}_i|^2 = \Bigg|\sqrt{\gamma N_{\text{r}} N_{\text{t}}}\alpha_0 \mathbf{w}_j^H \mathbf{a}_{\text{r}}(\theta_0)\mathbf{a}_{\text{t}}(\phi_0)^H \mathbf{f}_i + \sqrt{\gamma N_{\text{r}} N_{\text{t}}} \sum_{p=1}^{L-1} \alpha_p \mathbf{w}_j^H \mathbf{a}_{\text{r}}(\theta_p)\mathbf{a}_{\text{t}}(\phi_p)^H \mathbf{f}_i\Bigg|^2. \tag{13}$$

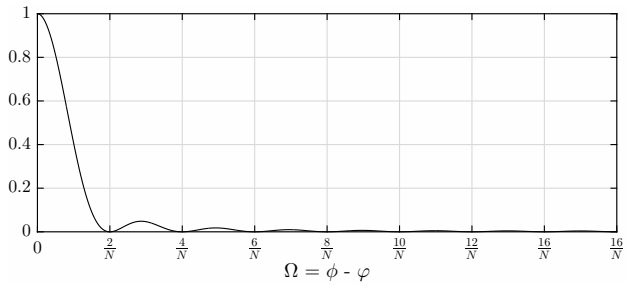

Fig. 2. Fejér kernel for N=16.

The previous expression can be bounded using the triangle identity [18, Ch. 15], with the upper bound given by

$$|\mathbf{w}_j^H \mathbf{H}\mathbf{f}_i|^2 \leq \gamma N_{\mathrm{r}} N_{\mathrm{t}} |\alpha_0|^2 |\mathbf{w}_j^H \mathbf{a}_{\mathrm{r}}(\theta_0)|^2 |\mathbf{a}_{\mathrm{t}}(\phi_0)^H \mathbf{f}_i|^2 + \gamma N_{\mathrm{r}} N_{\mathrm{t}} \sum_{p=1}^{L-1} |\alpha_p|^2 |\mathbf{w}_j^H \mathbf{a}_{\mathrm{r}}(\theta_p)|^2 |\mathbf{a}_{\mathrm{t}}(\phi_p)^H \mathbf{f}_i|^2, \quad (14)$$

whereas the lower bound reads

$$|\mathbf{w}_j^H \mathbf{H}\mathbf{f}_i|^2 \geq \gamma N_{\mathrm{r}} N_{\mathrm{t}} |\alpha_0|^2 |\mathbf{w}_j^H \mathbf{a}_{\mathrm{r}}(\theta_0)|^2 |\mathbf{a}_{\mathrm{t}}(\phi_0)^H \mathbf{f}_i|^2 - \gamma N_{\mathrm{r}} N_{\mathrm{t}} \sum_{p=1}^{L-1} |\alpha_p|^2 |\mathbf{w}_j^H \mathbf{a}_{\mathrm{r}}(\theta_p)|^2 |\mathbf{a}_{\mathrm{t}}(\phi_p)^H \mathbf{f}_i|^2. \quad (15)$$

Obviously, the non-sum term dominates. The square magnitude of the inner product of two beamforming vectors is

$$|\mathbf{a}(\phi)\mathbf{a}(\varphi)|^2 = \frac{1}{N^2} \left| \frac{\sin \frac{\pi(\phi-\varphi)N}{2}}{\sin \frac{\pi(\phi-\varphi)}{2}} \right|^2 := F_N(\phi - \varphi). \quad (16)$$

The term $F_N(\phi - \varphi)$ is the Fejér kernel of the order N [19], and it represents the beam pattern of an ULA (see Fig. 2).

As the other paths fall in far bins ($\Omega > 2/N$), the sum terms are negligible, thus we can express (15) as

$$|\mathbf{w}_j^H \mathbf{H}\mathbf{f}_i|^2 \approx \gamma N_{\mathrm{r}} N_{\mathrm{t}} |\alpha_0|^2 F_{N_r}(\theta_0 - \varphi_j) F_{N_t}(\phi_0 - \varphi_i). \quad (17)$$

For extremely large arrays (*i.e.* the Fejér kernel tends to 1 as $N \to \infty$) or when the beamforming directions are aligned with the AoA and AoD, (17) reads

$$|\mathbf{w}_j^H \mathbf{H}\mathbf{f}_i|^2 \approx \gamma N_{\mathrm{r}} N_{\mathrm{t}} |\alpha_0|^2. \quad (18)$$

Under the above assumption, after going through all beamforming vectors pairs, $|h_{\mathrm{eff}}|^2$ is obtained as follows

$$|h_{\mathrm{eff}}|^2 = \gamma N_{\mathrm{r}} N_{\mathrm{t}} \max\{|\alpha_0|^2, |\alpha_1|^2, ..., |\alpha_{L-1}|^2\}. \quad (19)$$

The effective channel is a random variable (RV) determined from L independent and identically distributed (i.i.d.) exponential RVs with a mean $\beta_p = N_{\mathrm{r}} N_{\mathrm{t}} \sigma_p^2$ using the max operation. Now, CDF and PDF can be derived in both NLoS and LoS scenarios.

1) CDF and PDF in an NLoS scenario: In an NLoS channel, all paths have the same variance $\sigma_p^2 = \sigma^2, p = 0, ..., L-1$. From (19), the RV $|h_{\mathrm{eff}}|^2$ is a max of L i.i.d. exponential RVs, having the equal mean of $\beta = \gamma N_{\mathrm{r}} N_{\mathrm{t}} \sigma^2$. The CDF is given by

$$F_{|h_{\mathrm{eff}}|^2}(x) = \left(1 - e^{-\frac{x}{\beta}}\right)^L, \quad (20)$$

which, after applying the binomial expansion, can be expressed as

$$F_{|h_{\mathrm{eff}}|^2}(x) = \sum_{l=0}^{L} (-1)^l \binom{L}{l} e^{-\frac{lx}{\beta}}. \quad (21)$$

By taking the derivative of (21), the PDF is obtained as

$$f_{|h_{\mathrm{eff}}|^2}(x) = \sum_{l=0}^{L} (-1)^{l+1} \binom{L}{l} \frac{l}{\beta} e^{-\frac{lx}{\beta}}. \quad (22)$$

Note that the PDF is zero for $l = 0$.

2) CDF and PDF in a LoS scenario: In a LoS channel, there is a dominant path with the power gain σ_0^2, while the other paths are weaker, having the variance $\sigma_p^2 = \sigma_0^2/A, p \neq 0$. Here, after the joint Tx/Rx beamforming, the LoS path is always chosen. The CDF of $|h_{\mathrm{eff}}|^2$ is given by

$$F_{|h_{\mathrm{eff}}|^2}(x) = \left(1 - e^{-\frac{x}{\beta_0}}\right) \left(1 - e^{-\frac{x}{\beta}}\right)^{L-1}, \quad (23)$$

where $\beta_0 = \gamma N_{\mathrm{r}} N_{\mathrm{t}} \sigma_0^2$ and $\beta = \beta_0/A$. After applying the binomial expansion, (23) reads

$$F_{|h_{\mathrm{eff}}|^2}(x) = \sum_{l=0}^{L-1} (-1)^l \binom{L-1}{l} e^{-\frac{lx}{\beta}} - \sum_{l=0}^{L-1} (-1)^l \binom{L-1}{l} e^{-\frac{x(l\beta_0+\beta)}{\beta_0\beta}}. \quad (24)$$

By taking the derivative of (24), the PDF is expressed as

$$f_{|h_{\mathrm{eff}}|^2}(x) = \sum_{l=0}^{L-1} (-1)^{l+1} \binom{L-1}{l} \frac{l}{\beta} e^{-\frac{lx}{\beta}} - \sum_{l=0}^{L-1} (-1)^{l+1} \binom{L-1}{l} (\frac{l}{\beta} + \frac{1}{\beta_0}) e^{-\frac{x(l\beta_0+\beta)}{\beta_0\beta}}. \quad (25)$$

Unlike the NLoS case, the PDF is nonzero for $l = 0$, and equals $f_{|h_{\mathrm{eff}}|^2}(x) = (L-1)/\beta_0 \exp(-x/\beta_0)$.

B. Capacity Analysis

We introduce substitute variables $x = |h_{\mathrm{eff}}|^2$, $c = \kappa^2$ and $d = \mathrm{SNR}_0{}^{-1}$, and express (11) as

$$R = \frac{1}{\ln 2} \left[\underbrace{\mathrm{E}\left\{ \ln\left(x\frac{c+1}{d} + 1 \right) \right\}}_{I_1} - \underbrace{\mathrm{E}\left\{ \ln\left(x\frac{c}{d} + 1 \right) \right\}}_{I_2} \right]. \quad (26)$$

Using the identity $\ln(ax+1) = G_{2,2}^{1,2}\left(ax|_{1,0}^{1,1}\right)$[1] [17], two expectations are

$$I_1 = \int_0^\infty G_{2,2}^{1,2}\left(\frac{c+1}{d} x|_{1,0}^{1,1} \right) f_x(x) dx, \quad (27)$$

$$I_2 = \int_0^\infty G_{2,2}^{1,2}\left(\frac{c}{d} x|_{1,0}^{1,1} \right) f_x(x) dx. \quad (28)$$

[1] $G_{p,q}^{m,n}\left(x|_{b_1,\ldots,b_q}^{a_1,\ldots,a_p}\right)$ is the Meijer's *G* function [18, Eq. 9.301]

In the NLoS scenario, by substituting (22) in (27) and (28), and with the help of [18, Eq. 7.813.1] and [18, Eq. 9.31.1], the ergodic capacity is derived as

$$R^{NLoS} = \frac{1}{\ln 2}\sum_{l=1}^{L}(-1)^{l+1}\binom{L}{l}\times \left\{G_{2,1}^{1,2}\left(\frac{\beta}{l}(1+\kappa^2)\mathrm{SNR}_0\big|_1^{1,1}\right) - G_{2,1}^{1,2}\left(\frac{\beta}{l}\kappa^2\mathrm{SNR}_0\big|_1^{1,1}\right)\right\}. \quad (29)$$

In the LoS scenario, the combination of (25), (27) and (28), results in four integrals that are solved with the help of [18, Eq. 7.813.1] and [18, Eq. 9.31.1]. The ergodic capacity reads

$$\begin{aligned} R^{LoS} = {} & \frac{L-1}{\ln 2}\left\{G_{2,1}^{1,2}\left(\beta_0(1+\kappa^2)\mathrm{SNR}_0\big|_1^{1,1}\right) - G_{2,1}^{1,2}\left(\beta_0\kappa^2\mathrm{SNR}_0\big|_1^{1,1}\right)\right\} + \frac{1}{\ln 2}\sum_{l=1}^{L-1}(-1)^{l+1}\binom{L-1}{l}\times \\ & \left\{G_{2,1}^{1,2}\left(\frac{\beta}{l}(1+\kappa^2)\mathrm{SNR}_0\big|_1^{1,1}\right) - G_{2,1}^{1,2}\left(\frac{\beta}{l}\kappa^2\mathrm{SNR}_0\big|_1^{1,1}\right) - G_{2,1}^{1,2}\left(\frac{\beta\beta_0}{l\beta_0+\beta}(1+\kappa^2)\mathrm{SNR}_0\big|_1^{1,1}\right) + G_{2,1}^{1,2}\left(\frac{\beta\beta_0}{l\beta_0+\beta}\kappa^2\mathrm{SNR}_0\big|_1^{1,1}\right)\right\}. \end{aligned} \quad (30)$$

Owing to [20, p. 229, eq. 5.1.20], $G_{2,1}^{1,2}\left(x\big|_1^{1,1}\right) = e^x E_1(x)$, which can be further bounded $0.5\ln(1+2/x) < G_{2,1}^{1,2}\left(x\big|_1^{1,1}\right) < \ln(1+1/x)$.

Eqs. (29) and (30) are exact in the case of extremely large arrays, where the Fejér kernel in (19) tends to one, or when the directions of beamforming vectors $\mathbf{f}$ and $\mathbf{w}$ are perfectly aligned with the AoD and AoA, respectively. The latter is only possible in the case of adaptive beamforming. However, typically, the transmitter and the receiver use a finite number of beamforming directions (codebook-based beamforming), so the perfect alignment is not always achieved. Nevertheless, even if the AoD/AoA do not fall at the center of a bin, but there is a random offset, the two expressions can be used if β and β_0 are scaled by a proper scaling factor. Intuitively, if the AoD and AoA are uniformly distributed within the bin, one can find the expected value of the Fejér kernel as

$$\mathrm{E}_\Omega\{F_N(\Omega)\} \approx \frac{2}{N}\int_0^{\frac{1}{N}} \mathrm{sinc}^2\left(\frac{\pi\Omega N}{2}\right)d\Omega = \frac{2}{\pi}\left(\mathrm{Si}(\pi) - \frac{2}{\pi}\right), \quad (31)$$

where $\mathrm{Si}(t)$ is the Sine integral [20, Eq. 5.2.1]. The expected value (≈ 0.77395) does not depend on the array size N and its square represents the scaling factor for β and β_0 in (29) and (30), which will be validated in the next section.

IV. Results

In this section, the simulation results are given and compared with the theory. We set $\kappa_t = \kappa_r = \{0.1, 0.3\}$ and $L = 5$. In the LoS channel, the LoS path has the average power of $\sigma_0^2 = 1$, whereas the remaining paths have a 10 dB smaller variance ($A = 10$), *i.e.* $\sigma_p^2 = 0.1$. The power normalization factor is $\gamma = A/\sigma_0^2(A + L - 1)$. In the NLoS channel, all paths have the same power of $\sigma_p^2 = 1$, hence $\gamma = 1/L$. AoDs and AoAs are uniformly distributed over $[-\pi/2, \pi/2]$. In the joint Tx/Rx beamforming, perfect alignment of the directions of transmit and receive beamforming vectors and the AoDs and AoAs of L paths is assumed. (This would be the case of adaptive beamforming). The process of selecting the best path is then described by (19). 5000 simulation runs are performed.

The ergodic capacity of a mmWave RF beamforming system with $N_t = N_r = 64$ antennas is plotted in Fig. 3, for both NLoS and LoS channel. A similar performance tendency is observed for both channels. In the high SNR region, the NLoS and LoS curves are overlapping and experiencing the same ceiling effect. From (11), the limit can be deduced as $C^\infty = \log_2(1 + (\kappa_t^2 + \kappa_r^2)^{-1})$. The curves differ only in the low SNR region.

For the NLoS channel, the impact of the array size on the ergodic capacity is depicted in Fig. 4. The result for the LoS channel is omitted due to space limitation, but a similar behavior is observed. Obviously, as the array size increases, the achievable capacity increases due to higher beamforming gains.

The results in the case of codebook-based beamforming are given in Fig. 5. Here, the transmit and receive beamforming vectors as defined in (12) are used in the joint Tx/Rx beamforming. Due to a limited number of beamforming directions ($N = N_t = N_r$ =64), the perfect alignment is not always achieved. Owing to our discussion in the last paragraph of Sec. III, the scaling factor from (31) is applied in (29) and

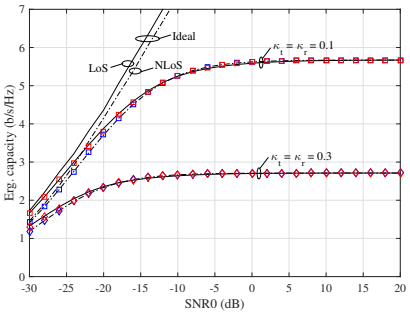

Fig. 3. The ergodic capacity in NLoS/LoS channels, $N_t = N_r = 64$. Solid lines are theoretical results in the NLoS case, and dotted ones refer to the LoS. Markers denote the simulation results (red - LoS, blue - NLoS).

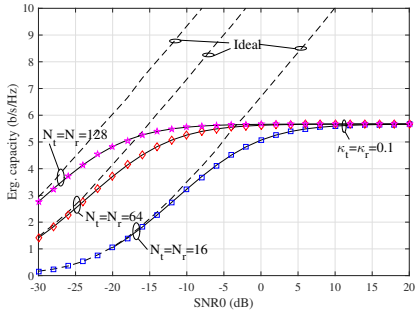

Fig. 4. The ergodic capacity in the NLoS channel for $N_t = N_r = (16, 64, 128)$. Solid lines represent the theoretical results, and markers denote the simulation results.

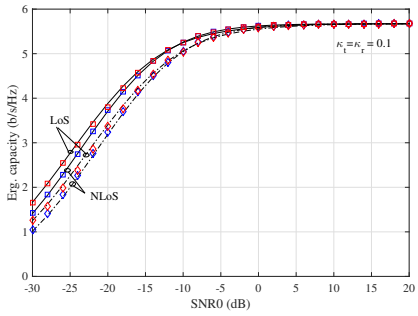

Fig. 5. The ergodic capacity in LoS and NLoS channels for $N_t = N_r = 64$. Solid lines are the theoretical results in the case of perfect alignment, whereas dashed lines represent the finite codebook-based alignment. Simulation results are denoted by markers (red - LoS, blue - NLoS).

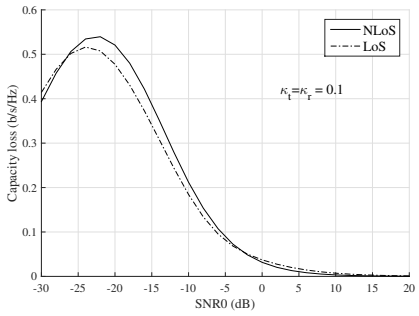

Fig. 6. The capacity loss due to the imperfect beam alignment (codebook-based vs. adaptive beamforming) in LoS and NLoS channels, for $N_t = N_r = 64$.

(30) to obtain the theoretical results. Also, the results are compared with those where the perfect alignment with the AoDs/AoAs is achieved (*i.e.* adaptive beamforming). It can be observed that the theoretical and the simulation results match very well, for both LoS and NLoS channels. Moreover, the codebook-based beamforming experiences a capacity loss when compared to the adaptive beamforming. Its origin is due to the imperfect alignment of the beamforming vectors and the AoD and AoA. The loss can be numerically calculated by finding the difference between capacities and is plotted for an example configuration in Fig. 6. For $N_t = N_r = 64$ and $\kappa_t = \kappa_r = 0.1$, the maximum capacity loss is reached at SNR of -22 dB for the NLoS and -24 dB for the LoS channel. For both channels, there is a similar capacity loss of almost 0.5 b/s/Hz at SNR ≈ -27 dB.

V. Conclusion

We have derived the closed-form analytical expressions of the ergodic capacity of millimeter wave (mmWave) radio-frequency (RF) beamforming systems in Line-of-Sight (LoS) and Non-Line-of-Sight (NLoS) channels. Our numerical study has revealed that the derived formulas are exact in the case of perfect beam alignment, while they are approximate, but with a high degree of accuracy, for codebook-based alignment. Moreover, the derived expressions take into account the impact of residual transceiver impairments on the ergodic capacity. The promising results present this work as a key tool for assessing the capacity of RF beamforming systems without the need to carry out exhaustive Monte-Carlo simulations.

References

[1] W. Roh, J.-Y. Seol, J. Park, B. Lee, J. Lee, Y. Kim, J. Cho, K. Cheun, and F. Aryanfar, "Millimeter-wave beamforming as an enabling technology for 5G cellular communications: theoretical feasibility and prototype results," *IEEE Commun. Mag.*, vol. 52, no. 2, pp. 106-113, 2014.

[2] T. Rappaport, R. W. Heath Jr., T. Daniels, and J. Murdock, *Millimeter wave wireless communications*, Prentice Hall, 2014.

[3] S. Hur, T. Kim, D. Love, J. Krogmeier, T. Thomas, and A. Ghosh, "Millimeter wave beamforming for wireless backhaul and access in small cell networks," *IEEE Trans. Commun.*, vol. 61, no. 10,pp. 4391-4403, 2013.

[4] O. E. Ayach, R. W. Heath, S. Abu-Surra, S. Rajagopal and Z. Pi, "The capacity optimality of beam steering in large millimeter wave MIMO systems," *in Proc. 13th International Workshop on Signal Processing Advances in Wireless Communications (SPAWC)*, 2012, pp. 100-104.

[5] Y. Li, S. He, C. Ma, S. Ma, C. Li and L. Yang, "Channel Characteristic and Capacity Analysis of Millimeter Wave MIMO Beamforming System," *in Proc. 83rd Vehicular Technology Conference (VTC Spring)*, 2016, pp. 1-5.

[6] A. Alkhateeb, O. El Ayach, G. Leus, and R. W. Heath, Jr., "Channel estimation and hybrid precoding for millimeter wave cellular systems," IEEE J. Sel. Topics Signal Process., vol. 8, no. 5, pp. 831–846, Oct. 2014.

[7] K. Hosoya et al, "Multiple sector ID capture (MIDC): A novel beamforming technique for 60-GHz band multi-Gbps WLAN/PAN systems," IEEE Trans. on Ant. and Prop., vol. 63, no. 1, pp. 81–96, Jan. 2015.

[8] M. E. Eltayeb, A. Alkhateeb, R. W. Heath and T. Y. Al-Naffouri, "Opportunistic beam training with hybrid analog/digital codebooks for mmWave systems," *in Proc. Global Conference on Signal and Information Processing (GlobalSIP)*, 2015, pp. 315-319.

[9] Z. Xiao, T. He, P. Xia and X. Xia, "Hierarchical Codebook Design for Beamforming Training in Millimeter-Wave Communication," in IEEE Transactions on Wireless Communications, vol. 15, no. 5, pp. 3380-3392, May 2016. doi: 10.1109/TWC.2016.2520930

[10] V. Va et al., "Beam tracking for mobile millimeter wave communication systems," in Proc. IEEE Int. Conf. Global Signal Process. (GlobalSIP), Dec. 2016, pp. 1–6.

[11] J. A. Zhang, X. Huang, V. Dyadyuk and Y. J. Guo, "Massive hybrid antenna array for millimeter-wave cellular communications," *IEEE Wireless Commun.*, vol. 22, no. 1, pp. 79-87, 2015.

[12] X. Yu, J.-C. Shen, J. Zhang, and K. B. Letaief, "Alternating minimization algorithms for hybrid precoding in millimeter wave MIMO systems," *IEEE J. Sel. Topics Signal Process.*, vol. 10, no. 3, pp. 485-500, 2016.

[13] N. Maletic, J. Gutierrez-Teran and E. Grass, "Beamforming mmWave MIMO: Impact of Nonideal Hardware and Channel State Information," 2018 26th Telecommunications Forum (TELFOR), Belgrade, 2018, pp. 1-6. doi: 10.1109/TELFOR.2018.8611829

[14] T. Schenk, *RF Imperfections in High-Rate Wireless Systems: Impact and Digital Compensation*, Springer, 2008.

[15] E. Bjornson, M. Matthaiou and M. Debbah, "A New Look at Dual-Hop Relaying: Performance Limits with Hardware Impairments," *IEEE Trans. Commun.*, vol. 61, no. 11, pp. 4512-4525, 2013.

[16] "Wireless LAN Medium Access Control (MAC) and Physical Layer (PHY) Specifications. Amendment 3: Enhancements for Very High Throughput in the 60 GHz Band," *IEEE Std. 802.11ad*, 2012.

[17] C. Zhong, M. Matthaiou, G. K. Karagiannidis and T. Ratnarajah, "Generic Ergodic Capacity Bounds for Fixed-Gain AF Dual-Hop Relaying Systems," in IEEE Transactions on Vehicular Technology, vol. 60, no. 8, pp. 3814-3824, Oct. 2011.

[18] I. S. Gradshteyn and I. M. Ryzhik, *Tables of Integrals, Series and Products*, 7th Ed., Elsevier, 2007.

[19] G. Lee, Y. Sung and M. Kountouris, "On the Performance of Random Beamforming in Sparse Millimeter Wave Channels," in IEEE Journal of Selected Topics in Signal Processing, vol. 10, no. 3, pp. 560-575, April 2016.

[20] M. Abramowitz and I. A. Stegun, *Handbook of Mathematical Functions*, New York: Dover, 1974.